ARTICLES
https://doi.org/10.1038/s41557-019-0413-8
nature chemistry

Electronic complementarity permits hindered butenolide heterodimerization and discovery of novel cGAS/STING pathway antagonists

Benjamin J. Huffman[1], Shuming Chen[2], J. Luca Schwarz[1], R. Erik Plata[1], Emily N. Chin[1], Luke L. Lairson[1*], K. N. Houk[2*] and Ryan A. Shenvi[1*]

sp^3-hybridized attached-rings are common motifs in secondary metabolites and represent tetrahedral equivalents to the biaryl substructures that overpopulate synthetic libraries. Few methods are available that can link fully substituted carbon atoms of two rings with stereocontrol. Here we have developed a stereoselective, heteroselective butenolide coupling that exhibits an unusually fast rate of C–C bond formation driven by exquisite complementarity of the reacting π systems. Heterodimerization generates a compound collection with topological complexity and diverse principal moments of inertia. The special status of the sp^3–sp^3 attached-ring motif is demonstrated in a high-throughput screen for inhibitors of the cyclic GMP-AMP synthase/stimulator of interferon genes pathway, which recruited these butenolide heterodimers from a field of 250,000 compounds. The driving forces underlying this general attached-ring coupling identify a novel paradigm for the accession of wider natural product chemical space, accelerating the discovery of selective lead compounds.

Molecular libraries play an integral role in drug development. Some libraries, however, are superior to others, as defined by their success in high-throughput screens or clinical progression[1]. Natural product-like attributes, earmarked as desirable[2,3], can lead to higher hit rates, higher selectivity[4] and lower toxicity-related attrition, whereas classically flat libraries show promiscuity[5]. Traditional synthetic libraries can be distinguished from natural product collections by their low number of stereocentres per molecule, high aromatic ring content and low fraction of sp^3-hybridized atoms (Fsp^3)[6,7]. With respect to ring connectivity (Fig. 1a), this difference is illustrated by the abundance in screening sets of biaryl motifs that are formed by sp^2–sp^2 cross-coupling methods (Fig. 1b)[8–10]. The tetrahedral equivalent (sp^3-hybridized attached-rings[5]) are instead found in collections of isolates (Fig. 1c). Synthetic libraries lack similar motifs because few methods can link fully substituted carbon atoms of two rings with stereocontrol[11,12]. This is occasionally referred to as the attached-ring problem[5,13–16].

We report an unusual butenolide dimerization that exhibits high heteroselectivity and high stereoselectivity. The reaction joins two distinct rings by a sigma bond between fully substituted carbons, yet exhibits an unusually high rate that outcompetes proton transfer, even from strong acids. Mechanistic interrogation reveals C–C bond formation to be non-rate-determining; computation suggests a very low energy barrier due to excellent alignment of secondary orbitals and stabilization by π–π stacking (Fig. 1d). In support of the idea that natural product character increases hit rate and specificity, butenolide heterodimers were identified as pathway-specific antagonists of cyclic GMP-AMP synthase (cGAS)/stimulator of interferon genes (STING) pathway, outcompeting ~250,000 other compounds in a high-throughput screen. This study exemplifies the close connection between natural product synthesis, reaction discovery and biological application.

Results and discussion

Recent total syntheses of jiadefenolide[17] and 11-*O*-debenzoyltashironin[18] featured a stereoselective Michael addition that was unusual in its fusion of different ring systems at the most-substituted positions (Fig. 1e). Although the γ-selective addition of butenolide anion[19] or siloxyfuran[20] to an electrophile was precedented, reaction between two substituted partners was not. β,β-Disubstitution of Michael acceptors can slow reaction rates by 6,000-fold or more[21], yet this reaction proceeded quickly even at −100 °C. The low barrier to the reaction and its outcompetition of other pathways raised questions that were not immediately answerable; for example, we assumed that the reaction proceeded by a standard Michael addition, but Kraus and Roth[19] proposed that reactions between less hindered systems might involve a Diels–Alder reaction and fragmentation (**4**, Fig. 1f). Indeed, we isolated only a hetero-Diels–Alder product (**3**) after acidic quench. Also, the reaction exhibited efficient conversion despite a potentially fast, competitive proton transfer from the electrophilic butenolide, which was calculated to be 10 pK_a units more acidic than the conjugate acid (Supplementary Fig. 17). One driving force for the reaction might have been strain release of **1** due to five sp^2 atoms embedded in its eight-atom, [3.3.0]-bicyclic framework. The reaction would not be general if bond formation were driven by strain.

The reaction instead proved to be very general. Products of direct, attached-ring coupling between prochiral 'electron-rich' butenolide nucleophiles and electron-deficient butenolide electrophiles are shown in Fig. 2a,b. Heterodimerizations to form these hindered attached-rings were diastereoselective and high yielding despite apparent steric congestion at the two participating carbon centres. Variations in structure (Fig. 2a,b) showed that even coupling partners bearing large alkyl groups at the site of bond formation (for example, isopropyl, cyclopropyl and cyclopentyl groups) surmounted the barrier to reaction. Strained bicyclic nucleophiles also underwent attached-ring coupling, enabling the rapid generation of

[1]Department of Chemistry, Scripps Research, La Jolla, CA, USA. [2]Department of Chemistry and Biochemistry, University of California, Los Angeles, CA, USA. *e-mail: llairson@scripps.edu; houk@chem.ucla.edu; rshenvi@scripps.edu

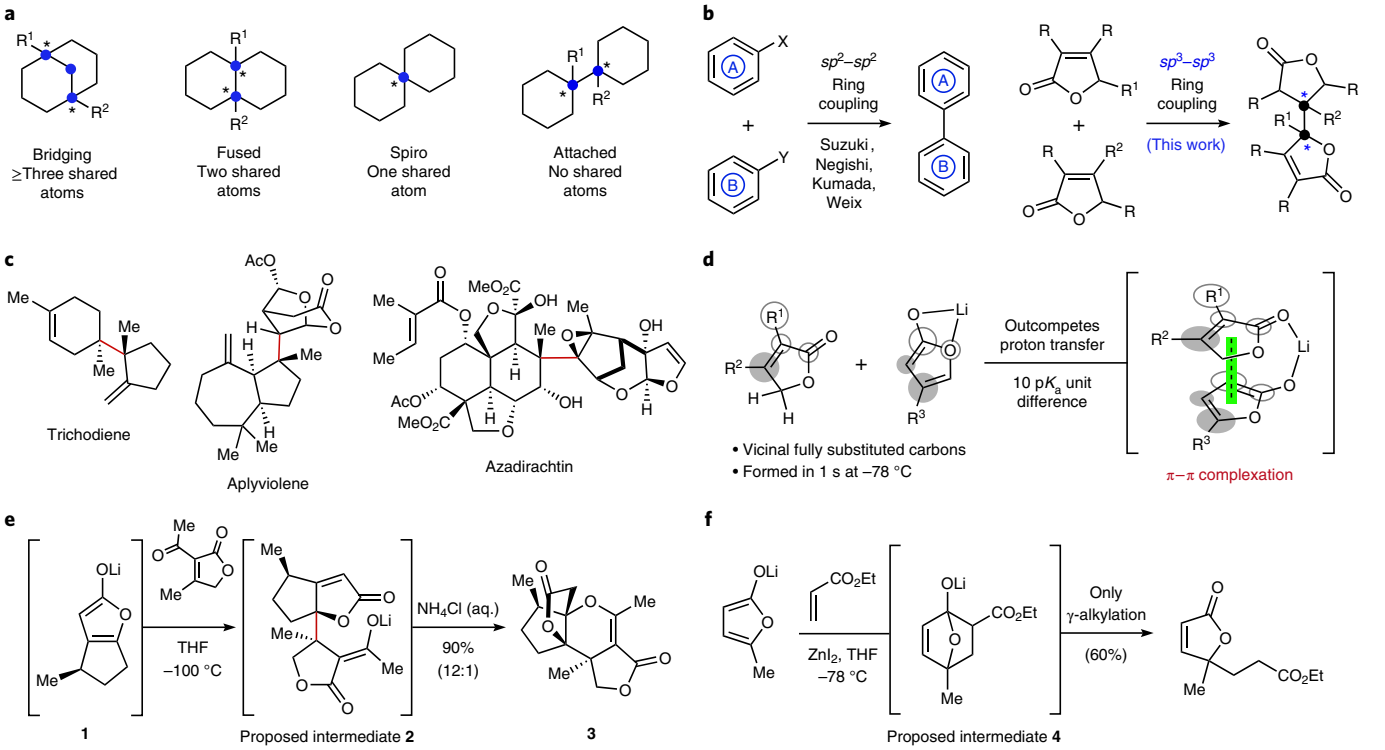

Fig. 1 | Attached rings bearing fully substituted bridgehead carbons are challenging motifs to form by direct intermolecular coupling. a, Of the four ring connectivity types, attached-rings share only electron density, not atoms. Control of stereochemistry by direct ring coupling does not benefit from a general stereochemical model. **b**, Biaryl rings can be combined using sp^2–sp^2 cross-coupling; here we show an example of a sp^3–sp^3 attached-ring synthesis. **c**, Examples of sp^3–sp^3 attached-rings that are representative of natural product chemical space. **d**, An example of how electronic complementarity can stabilize the transition state for attached-ring formation relative to alternative reactions. **e**, Initial observations of an unusually fast stereoselective butenolide heterodimerization. **f**, A proposed [4 + 2] mechanism for γ-selective butenolide Michael additions.

saturated, polycyclic systems that are characteristic of natural product chemical space. A range of electrophiles (Fig. 2b) also formed attached-ring products, with a focus on electronically differentiated β-aryl butenolides. The value of these substrates related to their use in a Hammett plot, principle moment of inertia (PMI) analysis and, we later discovered, their privileged activity in a pathway-targeted cell-based high-throughput screen. Mutually exclusive reactivity was observed between 'nucleophilic' and 'electrophilic' butenolides. As shown in Fig. 2c, both nucleophilic butenolide **5** and electrophilic butenolide **6** were completely unreactive with themselves, in contrast to unhindered butenolides, which readily homodimerize[19].

The formation of vicinal fully substituted centres was not limited to butenolide heterodimerization, but could be extended to both acyclic and cyclic α,β-unsaturated γ-ketoesters (Fig. 2d). Although either C2 or C3 can accept nucleophiles, reaction proceeded selectively at the more electron-deficient, but more hindered C2 position to form a quaternary carbon. However, a range of electrophiles proved completely unreactive (Fig. 2e), illustrating the unusual specificity of this reaction.

Formation of these hindered, fully substituted carbons between attached-rings proceeded under irreversible, basic conditions and at extremely high rates. To underscore this point, fast quenching experiments indicated bond formation was complete within 5 s under the standard conditions of Fig. 2 and even competed with proton transfer from 2 equiv. HCl that was pre-mixed with the electrophile (Fig. 3a, entry 3). The fast rate permitted formation of attached-ring product **7** in water/THF mixtures, despite use of a lithium enolate. Only competition against 10 equiv. of HCl completely suppressed product formation at –78 °C, allowing us to measure the reaction rate by rapid quench experiments.

Initially we attempted to define the rate using in situ infrared analysis (Fig. 3b), but the reaction completed in less than 1 s at 0.1 M, whereas the maximal signal was reached after 4 s using any analyte. As shown in the infrared trace, neither the addition of nucleophile to the electrophile nor the reverse addition provided a definitive infrared signal for the exogenous reagent, implying that both were consumed faster than detection, frustrating rate law determination (see page 66 of the Supplementary Information). These data at least provided a rate ceiling of a slowest bimolecular rate constant of $3.6 \pm 0.2\ M^{-1}\ s^{-1}$ ($t_{1/2} \leq 2.8$ s @ 0.1 M) and a highest free energy of activation ($\Delta G^{\ddagger}$) of 10.8 ± 0.1 kcal mol^{-1}. Next, we turned to rapid injection/rapid quench at high dilution. Two 0.1 M solutions of 0.01 mmol **5·Li** and **6** were simultaneously injected into 100 ml of THF at –78 °C, equivalent to a 100 μM final concentration of reaction. After 5 s, methanolic HCl was injected (10 equiv. <1 s), followed by 1,3,5-trimethoxybenzene as an internal standard. Quadruplicate replication of this experiment delivered a yield of 73% ± 8, corresponding to a model bimolecular rate constant of $5.4 \times 10^3\ M^{-1}\ s^{-1}$, a $t_{1/2}$ of 1.9 sec at 100 μM and a free energy of activation of 7.9 ± 0.2 kcal mol^{-1} at –78 °C (replication at 20 μM produced similar values, Fig. 3c). These rates provided a maximum energy barrier for a bimolecular reaction, although the extremely fast kinetics prohibited rate law determination. However, the rate constant stood out as unusual for a disubstituted lithium enolate and a β,β-disubstituted Michael acceptor. For comparison, the aldol addition of 4-fluoroacetophenone lithium enolate dimer to benzaldehyde at –120 °C exhibited a bimolecular rate constant of about $5\ M^{-1}\ s^{-1}$ (ref. [22]), prompting the question of why more hindered partners reacted at such high rates.

One answer might be an orthogonal reaction pathway, such as the one Kraus' proposed for Diels–Alder cycloaddition/fragmentation.

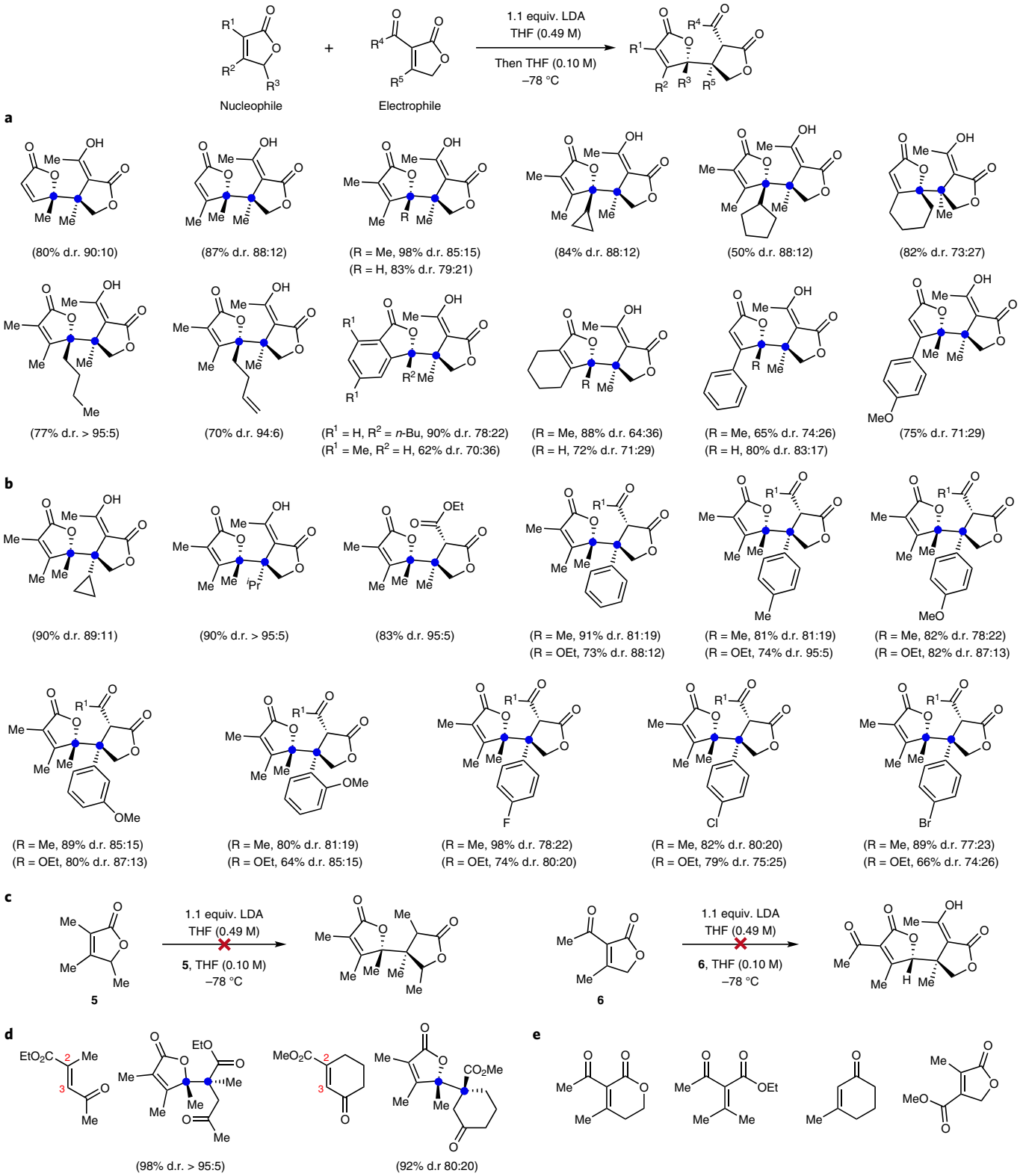

Fig. 2 | Vicinal fully substituted stereocentres from butenolide heterodimerization. a, Variations of the nucleophile. **b**, Variations of the electrophile. **c**, Neither **5** nor **6** are self-reactive, showing their heterospecificity. **d**, Proof-of-principle for the extension of the buteneolide heterodimerization to other coupling partners (shown). **e**, A range of electrophiles demonstrate how subtle changes in structure ablate reactivity. d.r., diastereomeric ratio; LDA, lithium diisopropylamide.

We turned to heavy atom kinetic isotope effect (KIE) experiments to probe this possibility: if a direct Michael addition were operative in the rate-determining step, a primary KIE would be observed at C_{4N} and C_{3E}, whereas a Diels–Alder/fragmentation mechanism would either produce a primary KIE at C_{1N}, C_{4N}, C_{2E} and C_{3E} (cycloaddition), or just C_{1N} and C_{2E} (fragmentation, see Fig. 3d). We measured

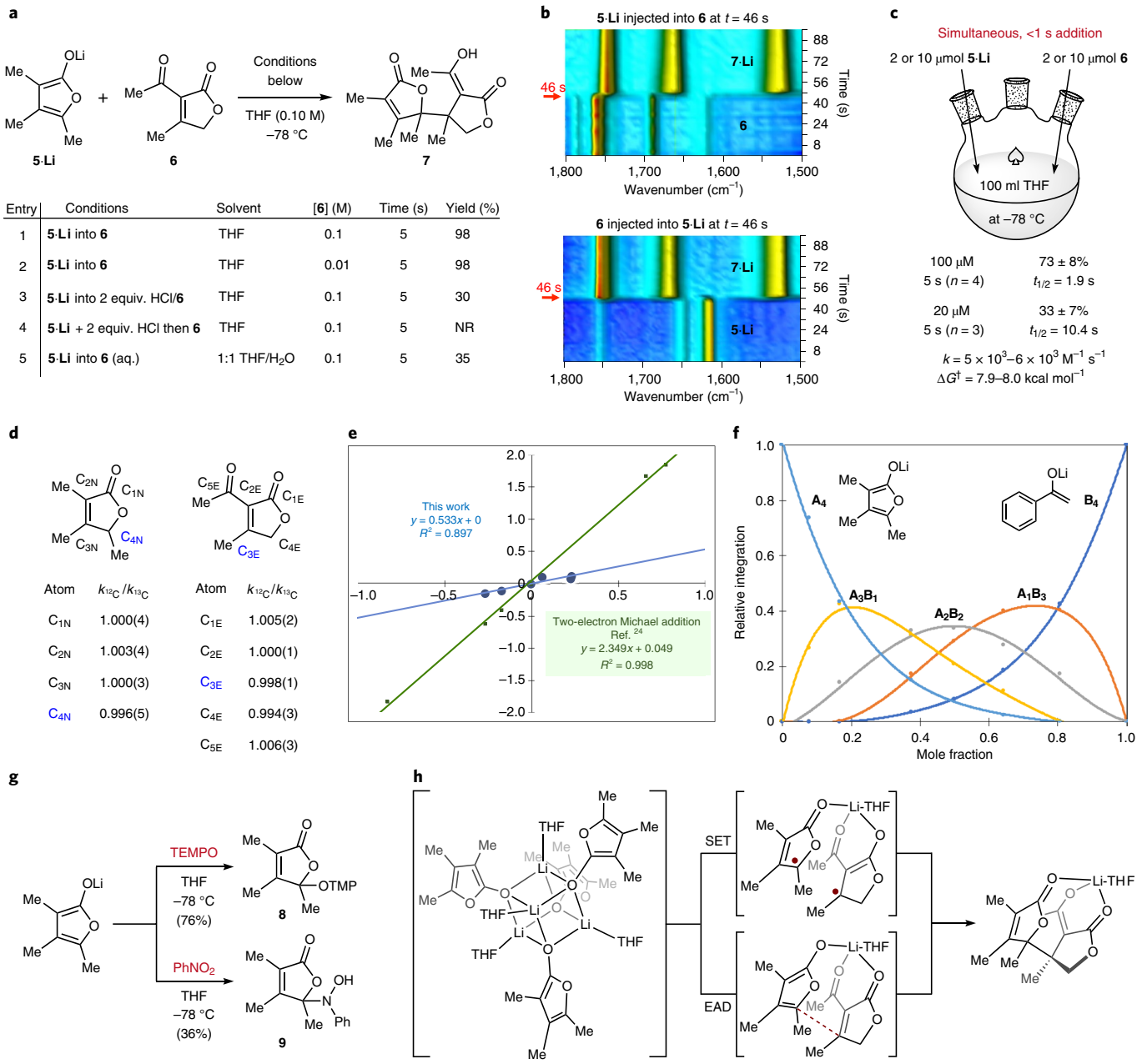

Fig. 3 | Kinetics data excludes C–C bond formation as rate determining. a, Hindered bond formation outcompetes proton transfer from Brønsted acids ($n=1$, entries 1–5). **b**, In situ infrared monitoring ($n=1$) shows that the reaction rate exceeds the scan rate. **c**, Rapid quench experiments at high dilution ($n=4$, 3) identify an extremely fast rate. **d**, ^{13}C KIEs near unity ($n=2$, C_{1N}–C_{4N}; $n=1$, C_{1E}–C_{5E}) exclude C–C bond formation as rate determining. **e**, A small, positive Hammett slope ($n=3$) excludes lithium coordination as rate determining. **f**, Enolate **5·Li** exists primarily as a cubic tetramer according to Collum's ^{6}Li Job plot analysis. **g**, Reaction of butenolide nucleophile with single-electron oxidants. **h**, Hypothesized mechanisms based on observed reactivity, rates and speciation. NR, no reaction; SET, single-electron transfer; EAD, electrophile-assisted deaggregation; TEMPO, (2,2,6,6-tetramethylpiperidin-1-yl)oxyl. $n=$X independent experiments.

^{13}C KIEs ($k_{^{12}C/^{13}C}$) at natural abundance using Singleton's method for high-precision measurement by NMR[23] and were surprised to find that the KIEs were near unity at all of the carbon atoms on both the electrophile and nucleophile; C–C bond formation is therefore not the rate-determining step and the energy barrier for attached-ring formation is even lower than the maximum value determined by rapid quench.

Three competing hypotheses were considered to explain these data. First, Li^+ coordination could be rate determining. If this were the case, electron-rich electrophiles should outcompete electron-deficient electrophiles. Instead, a Hammett plot indicated the opposite (Fig. 3e). The positive ρ-value of 0.53, albeit small, is inconsistent with coordination as rate-determining but also diverges from observations on analogous systems such as diethylmalonate anion additions to β-aryl Michael acceptors ($\rho=2.35$)[24]. A second hypothesis is that single electron transfer (SET) is rate-determining, before subsequent rapid C–C bond formation. Previous work suggested that aldol and Michael additions with low ρ-values and no $k_{^{12}C/^{13}C}$ KIEs at the reacting carbons indicated SET as an elementary step; indeed, **5·Li** underwent productive reaction with radical

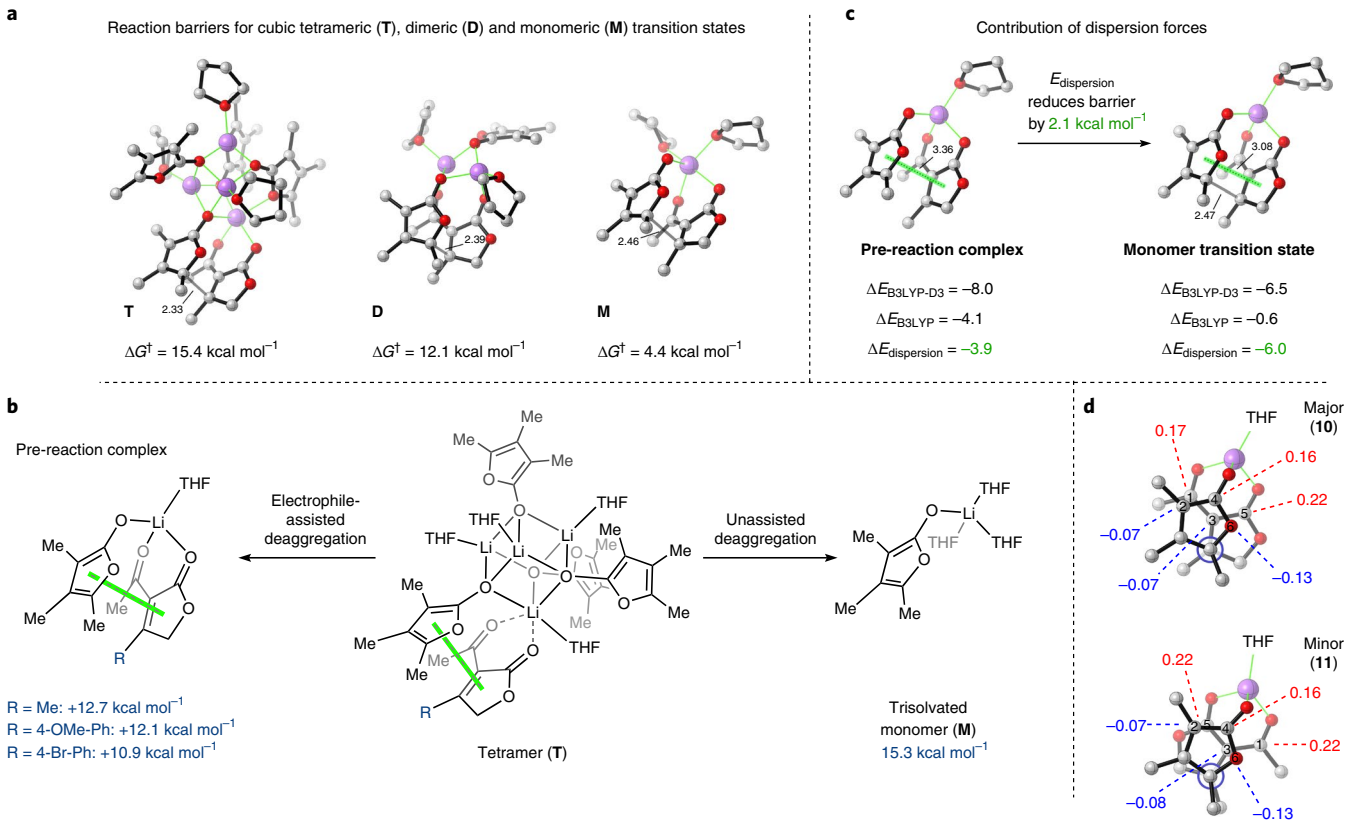

Fig. 4 | Calculation of aggregate reaction barriers and deaggregation energies. a, Calculated free energies of activation for Michael addition transition states with different aggregation levels at the ωB97XD/6-311++G(d,p), SMD (THF)//ωB97XD/6-31G(d), SMD (THF) level of theory. **b**, Calculated free-energy changes following tetramer deaggregation with and without the assistance of an electrophile at the ωB97XD/6-311++G(d,p), SMD (THF) // ωB97XD/6-31G(d), SMD (B3LYP/6-311G(d,p)), SMD(THF) level of theory. **c**, Dispersive interactions reduce the energy barrier by 2.1 kcal mol^{-1}. **d**, Calculated Hirshfeld charges at the ωB97XD/6-31G(d), SMD (THF) level of theory.

traps such as TEMPO (**8**) and nitrobenzene (**9**) at −78 °C, probably through a stabilized radical (Fig. 3g). SET could explain the heterospecificity, high rate and temperature-independent diastereoselectivity (see page 77 of the Supplementary Information). Density functional theory calculations, however, showed that SET processes are endergonic (Supplementary Scheme 1). Attempts to locate open-shell transition states with a variety of density functionals predicted that only closed-shell structures are significantly more stable than open-shell diradical structures, further indicating that radical pathways are unfavourable.

Our third hypothesis is that an aggregation state change is rate determining. This mechanism would fit the near-unity $k_{^{12}C/^{13}C}$ KIE. Lithium enolate **5·Li** was determined to exist primarily as its cubic tetramer using the method of continuous variation (Job plot), as pioneered by Collum (^{6}Li NMR, −78 °C; Fig. 3f). We computed transition states for C–C bond formation involving mono-, di- and tetrameric lithium enolates, but only the monomer exhibited an energy barrier consistent with experimental rates (see Fig. 4 for energetics). Remarkably, the reaction between lithium enolate monomer and a Li$^+$-chelated electrophile exhibited an energy barrier of only 4.4 kcal mol^{-1}, which is consistent with its absence in the rate-determining step. The high-energy process in the overall reaction pathway seems to be the dissociation of a cubic tetramer of lithium enolate. The thermodynamics of this dissociation becomes more favourable with participation of the bidentate electrophile, which can complex the nucleophile through π-interactions (strengthened with electron-withdrawing substituent, Fig. 4b). These data fit the Hammett plot, and energies now begin to approach the observed reaction barrier. Remarkably, it seems that π-complexation and not Li$^+$ coordination causes deaggregation; furthermore, both theory and experiment indicate that C–C bond formation is extremely favourable and very sensitive to structure (Fig. 2e, Supplementary Scheme 1 and Supplementary Fig. 16): the butenolide pairs are exquisitely matched to react, whereas small perturbations cause failure. What is the basis for this unusual specificity?

One idiosyncrasy of this system involves the intimate and stabilizing π–π interactions between the conjugated systems of the two reacting partners (Fig. 4). The π–π stacking in non-polar systems is often controlled primarily by dispersion interactions, whereas polar substituents can introduce electrostatic stabilization as well[25]. In the case of the pre-reaction complex and transition states (Fig. 4c), dispersion, secondary orbital interactions and electrostatics between the complementary HOMO–LUMO orbitals and charges of electrophile and nucleophile lead to a considerably reduced energy barrier. We compared the activation electronic energy (ΔE) of the Michael addition step calculated using the dispersion-corrected B3LYP-D3 and uncorrected B3LYP functionals to estimate the magnitude of dispersion stabilization. A pre-reaction π–π stacked complex of nucleophile and electrophile is stabilized by dispersive interactions, which proved stronger in the transition state than in the pre-reaction complex, resulting in an overall reduction of the barrier by 2.1 kcal mol^{-1}. The electronically biased butenolides are almost perfectly predisposed to react due to ideal electronic complementarity between nucleophile and electrophile; minor deviations from these ideal interactions lead to prohibitively high energy barriers (compare with Fig. 2e). In these cases, proton transfers outcompete C–C bond formation.

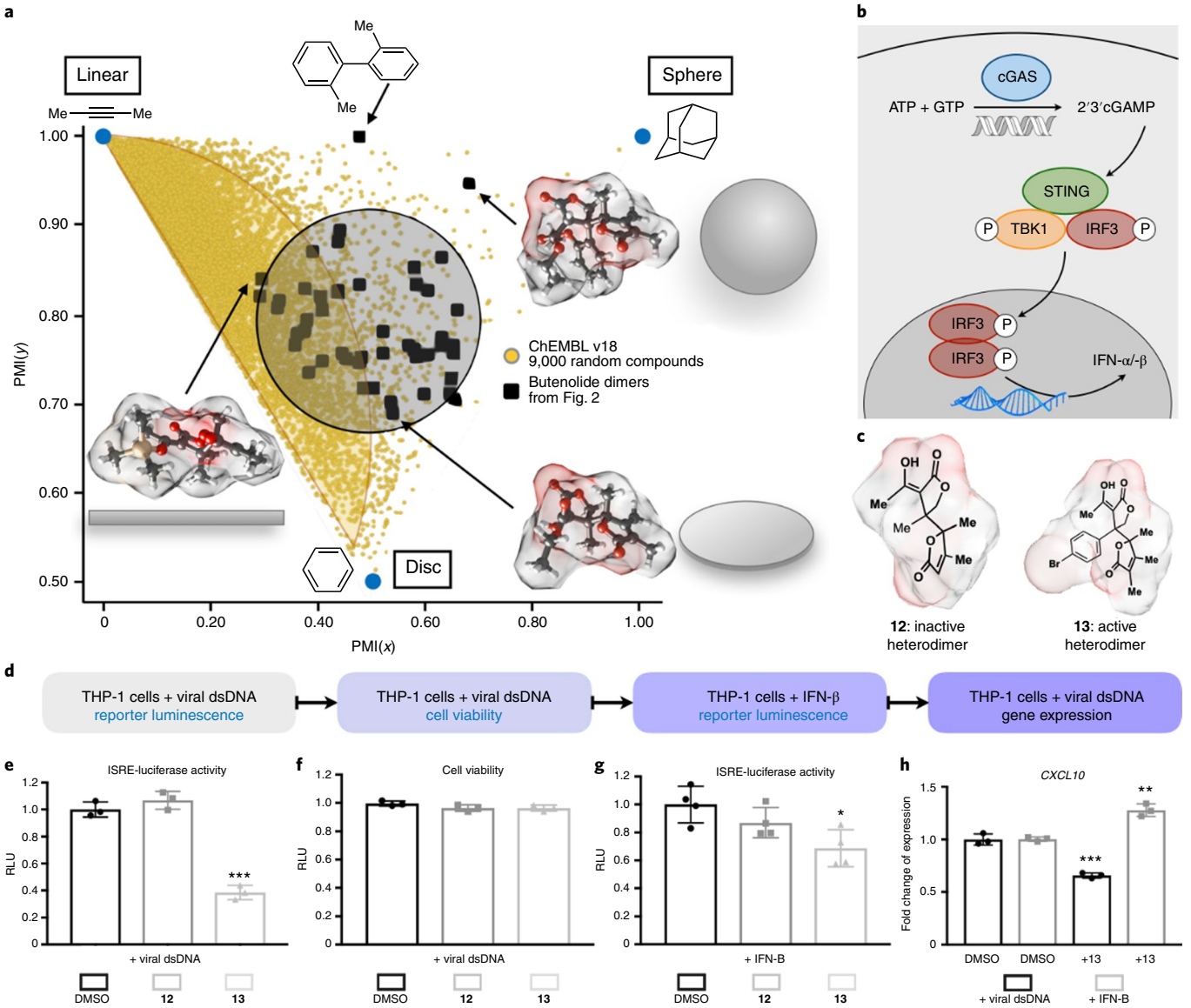

Fig. 5 | Identification of butenolide heterodimer-based cGAS-STING pathway inhibitors from a cell-based chemical screen. a, A comparison of the PMI between a representative section of ChEMBL database and attached-ring dimers in Fig. 2. Panel adapted with permission from ref. [8], American Chemical Society. **b**, A schematic representation of the cGAS/STING pathway. **c**, The structure of one identified screening hit (**13**) and a representative dead analogue (**12**). **d**, The workflow from HTS to validation. **e**, IRF-inducible luciferase activity was measured in human THP-1 cells co-treated with viral dsDNA oligonucleotide and either compound (15 μM) or vehicle (DMSO) ($n = 3$). **f**, Cell viability was assessed using cell titre Glo assay under the same treatment conditions to negate false-positive hits due to cytotoxicity ($n = 3$). **g**, Pathway specificity was evaluated by measuring IRF-luciferase activity in response to co-treatment with downstream activator, IFN-B and compound ($n = 4$). **h**, Gene expression analysis of an ISRE-driven target gene, CXCL10, was evaluated in response to treatment with **13** and viral dsDNA or IFN-B ($n = 3$). All data are the mean ± s.d. $^*P \leq 0.05$, $^{**}P \leq 0.01$, $^{***}P \leq 0.001$, as analysed by two-tailed Student's *t*-test. $n = X$ number of independent experiments. HTS, high-throughput screening; TBK1, TANK-binding kinase 1; IFN, interferon; RLU, relative luminometer units.

This electronic complementarity also explains trends in diastereoselectivity (Fig. 4d), with contributions from both attractive and repulsive electronic effects (closed-shell repulsion that is unfavourable in eclipsed transition states). The major (**10**) diastereomeric transition state exhibits superior HOMO–LUMO and charge alignment, where three favourable orbital and electrostatic interactions exist between the two reacting partners (C1–C2, C3–C4, C5–O6). The minor (**11**) diastereomeric transition state substantially disrupts this alignment and also possesses unfavourable eclipsing interactions about the forming C–C bond (Fig. 4d).

The value of this butenolide heterodimerization and the small library displayed in Fig. 2 derived from its orthogonality in chemical space to existing synthetic compound collections. Unlike many synthetic libraries, the butenolide heterodimers have a large number of stereocentres per heavy atom (15% for model **7**), low aromatic ring content, high Fsp^3, high ring content, high oxygen content and low nitrogen content[7]. The PMI metric used to evaluate library shape diversity distinguished the butenolide heterodimers from the ChEMBL database of bioactive molecules developed by the European Bioinformatics Institute[26] (Fig. 5a also includes diversifications of compound **7**, see page 84 of the Supplementary Information). Compounds in the ChEMBL database were largely linear or flat (typical of combinatorial synthetic collections), whereas the heterodimers populated a diverse shape space,

including highly spherical motifs. As a result, the butenolide dimers of Fig. 2 were collected by the California Institute for Biomedical Research (Calibr) and added to high throughput screens for therapeutically relevant targets.

Four butenolide heterodimers (including compound **13**) were identified as hits from a cGAS/STING pathway-targeted cell-based phenotypic chemical screen of ~250,000 compounds. The cGAS/STING pathway is an evolutionarily conserved pattern recognition mechanism, which serves as a sensor for cytosolic nucleic acid derived from invading pathogens. In response to double stranded DNA, cGAS becomes activated to generate the cyclic dinucleotide cyclic GMP-AMP (cGAMP), which is recognized by STING and serves to initiate TBK1/IRF3-dependent interferon-stimulated gene expression (Fig. 5b), thereby stimulating innate and adaptive immune response mechanisms[27,28]. Mislocalized cytosolic self-DNA also leads to aberrant cGAS activation, which is thought to play a causative role in autoimmunity disorders[29]. The ability of **13** to inhibit cGAS/STING pathway activation was identified from a screen involving human THP1 cells, harbouring an IRF-inducible reporter construct (THP1-ISRE-Luciferase), transiently transfected with viral dsDNA. Secondary assays, based on cell viability and direct versus secondary pathway selectivity (that is IFNβ1 stimulation), were used to identify pathway-selective non-toxic hits (Fig. 5d). Importantly, the physiological relevance of **13** was demonstrated by its observed ability to reduce mRNA levels of *CXCL10*, a critcally important indicator of interferon-stimulated gene expression, in dsDNA-stimulated THP1 cells at non-toxic concentrations in a cGAS-STING pathway selective manner (Fig. 5e–h). Preliminary SAR analysis involving 21 butenolide dimers (see page 87 of the Supplementary Information) revealed a clear trend consistent with specific site binding and also enabled the identification of an inactive analogue (**12**), which served as a negative control for the chemotype. Rapid identification of **13** as a lead for inhibition of the cGAS/STING pathway substantiates in a compelling way the value of attached-ring motifs within natural product space.

Conclusion

The continued value of natural products derives from the chemical space they inhabit. In contrast to large combinatorial libraries, natural product space tends to include more hydroxyl groups, sp^3-hybridized atoms, rings and stereocentres, and a more spherical principal moment of inertia[1,7,11]. Synthetic libraries are overpopulated with molecules that are easy to synthesize, but their quantity does not always translate to quality[9]. A lack of stereochemistry, high planarity and high aromatic character can deliver 'local minima' leads: low-quality hits that suffer high attrition rates due to promiscuity and toxicity[6–10]. Although natural product-like space is statistically advantageous for lead identification, it is less synthetically accessible and largely absent from synthesized screening sets[30]. Facile access to natural product motifs, however, can alter the overall properties of synthetic libraries[31]. We have demonstrated a stereoselective synthesis of fully substituted attached-ring motifs driven by near-perfect electronic complementarity of the reactants. The small library of compounds diverges from the chemical space inhabited by large synthetic libraries according to PMI analysis. The value of this small collection was demonstrated in a high-throughput screen for inhibitors of the cGAS/STING pathway. Heterodimer **13** was recruited from a field of 250,000 compounds and identified as a pathway-selective non-toxic hit for deployment against autoimmunity disorders. Identification of a stereoselective, heteroselective attached-ring coupling opens the door to a rational, mechanistically driven solution to the attached-ring problem and structural expansions along two proximal tetrahedral vector sets. A search for viable coupling partners and design principles is now underway. We anticipate that similar electronically complementary coupling reactions will extend into areas of chemical space not typically reached by synthetic methods or bioorthogonal reactions. Our aim is to render these types of reactions combinatorial, blurring the line between synthetic and natural product space to harness the power of nature's chemicals.

Online content

Any Nature Research reporting summaries, source data, extended data, supplementary information, acknowledgements, peer review information; details of author contributions and competing interests; and statements of data and code availability are available at https://doi.org/10.1038/s41557-019-0413-8.

Received: 12 July 2018; Accepted: 13 December 2019;
Published online: 10 February 2020

References

1. Leeson, P. D. & Springthorpe, B. The influence of drug-like concepts on decision-making in medicinal chemistry. *Nat. Rev. Drug. Discov.* **6**, 881–890 (2007).
2. Ertl, P., Roggo, S. & Schuffenhauer, A. Natural product-likeness score and its application for prioritization of compound libraries. *J. Chem. Inf. Model.* **48**, 68–74 (2008).
3. Lovering, F., Bikker, J. & Humblet, C. Escape from flatland: increasing saturation as an approach to improving clinical success. *J. Med. Chem.* **52**, 6752–6756 (2009).
4. Clemons, P. A. et al. Small molecules of different origins have distinct distributions of structural complexity that correlate with protein-binding profiles. *Proc. Natl Acad. Sci. USA* **107**, 18787–18792 (2010).
5. Lovering, F. Escape from Flatland 2: complexity and promiscuity. *ChemMedChem* **4**, 515–519 (2013).
6. Feher, M. & Schmidt, J. M. Property distributions: differences between drugs, natural products, and molecules from combinatorial chemistry. *J. Chem. Inf. Comput. Sci.* **43**, 218–227 (2003).
7. Lachance, H., Wetzel, S., Kumar, K. & Waldmann, H. Charting, navigating, and populating natural product chemical space for drug discovery. *J. Med. Chem.* **55**, 5989–6001 (2012).
8. Brown, D. G. & Boström, J. Analysis of past and present synthetic methodologies on medicinal chemistry: where have all the new reactions gone? *J. Med. Chem.* **59**, 4443–4458 (2016).
9. Brown, D. G., Gagnon, M. M. & Boström, J. Understanding our love affair with *p*-chlorophenyl: present day implications from historical biases of reagent selection. *J. Med. Chem.* **58**, 2390–2405 (2015).
10. Ritchie, T. J. & Macdonald, S. J. F. The impact of aromatic ring count on compound developability—are too many aromatic rings a liability in drug design? *Drug Discov. Today* **14**, 1011–1020 (2009).
11. Choi, J. & Fu, G. C. Transition metal–catalyzed alkyl–alkyl bond formation: another dimension in cross-coupling chemistry. *Science* **356**, 152–160 (2017).
12. Overman, L. E. & Velthuisen, E. J. Scope and facial selectivity of the prins-pinacol synthesis of attached rings. *J. Org. Chem.* **71**, 1581–1587 (2006).
13. Daub, M. E., Prudhomme, J., Le Roch, K. & Vanderwal, C. D. Synthesis and potent antimalarial activity of kalihinol B. *J. Am. Chem. Soc.* **137**, 4912–4915 (2015).
14. Tang, Z. et al. Highly enantioselective synthesis of bisoxindoles with two vicinal quaternary stereocenters via Lewis base mediated addition of oxindoles to isatin-derived ketimines. *Org. Biomol. Chem.* **12**, 6085–6088 (2014).
15. Fuchs, J. R. & Funk, R. L. Total synthesis of (±)-perophoramidine. *J. Am. Chem. Soc.* **126**, 5068–5069 (2004).
16. Movassaghi, M., Ahmad, O. K. & Lathrop, S. P. Directed heterodimerization: stereocontrolled assembly via solvent-caged unsymmetrical diazene fragmentation. *J. Am. Chem. Soc.* **133**, 13002–13005 (2011).
17. Lu, H.-H., Martinez, M. D. & Shenvi, R. A. An eight-step gram-scale synthesis of (–)-jiadifenolide. *Nat. Chem.* **7**, 604–607 (2015).
18. Ohtawa, M. et al. Synthesis of (–)-11-*O*-debenzoyltashironin: neurotrophic sesquiterpenes cause hyperexcitation. *J. Am. Chem. Soc.* **139**, 9637–9644 (2017).
19. Kraus, G. A. & Roth, B. Michael addition reactions of angelica lactone. *Tetrahedron Lett.* **18**, 3129–3132 (1977).
20. Chabaud, L., Jousseaume, T., Retailleau, P. & Guillou, C. Vinylogous Mukaiyama–Michael reactions between 2-silyloxyfurans and cyclic enones or unsaturated oxo esters. *Eur. J. Org. Chem.* **2010**, 5471–5481 (2010).
21. Jackson, P. A., Widen, J. C., Harki, D. A. & Brummond, K. M. Covalent modifiers: a chemical perspective on the reactivity of α,β-unsaturated carbonyls with thiols via hetero-Michael addition reactions. *J. Med. Chem.* **60**, 839–885 (2017).

22. Kolonko, K. J., Wherritt, D. J. & Reich, H. J. Mechanistic studies of the lithium enolate of 4-fluoroacetophenone: rapid-injection NMR study of enolate formation, dynamics, and aldol reactivity. *J. Am. Chem. Soc.* **137**, 16774–16777 (2011).
23. Singleton, D. & Thomas, A. High-precision simultaneous determination of multiple small kinetic isotope effects at natural abundance. *J. Am. Chem. Soc.* **117**, 9357–9358 (1995).
24. Kaumanns, O., Lucius, R. & Mayr, H. Determination of the electrophilicity parameters of diethyl benzylidenemalonates in dimethyl sulfoxide: reference electrophiles for characterizing strong nucleophiles. *Chem. Eur. J.* **14**, 9675–9682 (2008).
25. Wheeler, S. E. & Houk, K. N. Substituent effects in the benzene dimer are due to direct interactions of the substituents with the unsubstituted benzene. *J. Am. Chem. Soc.* **130**, 10854–10855 (2008).
26. Gaulton, A. et al. The ChEMBL database in 2017. *Nucleic Acids Res.* **45**, D945–D954 (2017).
27. Sun, L., Wu, J., Du, F., Chen, X. & Chen, Z. Cyclic GMP-AMP synthase is a cytosolic DNA sensor that activates the type i interferon pathway. *Science* **339**, 786–791 (2013).
28. Cai, X., Chiu, Y.-H. & Chen, Z. J. The cGAS-cGAMP-STING pathway of cytosolic DNA sensing and signaling. *Mol. Cell* **54**, 289–296 (2014).
29. Crow, Y. J. & Manel, N. Aicardi–Goutières syndrome and the type I interferonopathies. *Nat. Rev. Immunol.* **15**, 429–440 (2015).
30. Wetzel, S., Schuffenhauer, A., Roggo, S., Ertl, P. & Waldmann, H. Cheminformatic analysis of natural products and their chemical space. *Chimia* **61**, 355–360 (2007).
31. Huffman, B. J. & Shenvi, R. A. Natural products in the marketplace: interfacing synthesis and biology. *J. Am. Chem. Soc.* **141**, 7709–7714 (2019).

Reporting summary. Further information on research design is available in the Nature Research Reporting Summary linked to this article.

Data availability

All data generated or analysed during this study are included in this Article and its Supplementary Information. Other data that support the findings in this study include crystallographic data deposited with the Cambridge Crystallographic Data Centre under accession nos. CCDC 1849246 (compound **SI-86**), 1849245 (compound **SI-46 minor**), 1849244 (compound **SI-46 major**), 1849243 (compound **SI-67**), 1849242 (compound **SI-93**) and 1849241 (compound **SI-66**).

Acknowledgements

We thank D.-H. Huang and L. Pasternack for NMR analysis, C. Moore and A. L. Rheingold for X-ray crystallographic analysis, H. M. Petrassi for PMI analysis and the ACS for use of data from ref. [1]. We thank D. L. Boger for helpful discussions. Financial support for this work was provided by the NSF (NSF Graduate Research Fellowships Program to B.J.H., CHE-1352587 and CHE-1856747 to R.A.S., and CHE-1764328 to K.N.H.). All calculations were performed on the Hoffman2 cluster at the University of California, Los Angeles and the Extreme Science and Engineering Discovery Environment (XSEDE) supported by the NSF (OCI-1053575).

Author contributions

B.J.H. and R.A.S. conceived the work, all authors designed the experiments, B.J.H., R.E.P., J.L.S. and E.N.C. performed the experiments. S.C. performed the calculations. All authors contributed to analysis of the data and composition of the manuscript.

Competing interests

A provisional patent has been submitted: US serial no. 62/776,306.

Additional information

Supplementary information is available for this paper at https://doi.org/10.1038/s41557-019-0413-8.

Correspondence and requests for materials should be addressed to L.L.L., K.N.H. or R.A.S.

Reprints and permissions information is available at www.nature.com/reprints.

nature research

Corresponding author(s): Lairson, Houk, Shenvi

Last updated by author(s): Sep 12, 2019

Reporting Summary

Nature Research wishes to improve the reproducibility of the work that we publish. This form provides structure for consistency and transparency in reporting. For further information on Nature Research policies, see Authors & Referees and the Editorial Policy Checklist.

Statistics

For all statistical analyses, confirm that the following items are present in the figure legend, table legend, main text, or Methods section.

n/a	Confirmed
☐	☒ The exact sample size (*n*) for each experimental group/condition, given as a discrete number and unit of measurement
☐	☒ A statement on whether measurements were taken from distinct samples or whether the same sample was measured repeatedly
☐	☒ The statistical test(s) used AND whether they are one- or two-sided *Only common tests should be described solely by name; describe more complex techniques in the Methods section.*
☐	☒ A description of all covariates tested
☒	☐ A description of any assumptions or corrections, such as tests of normality and adjustment for multiple comparisons
☐	☒ A full description of the statistical parameters including central tendency (e.g. means) or other basic estimates (e.g. regression coefficient) AND variation (e.g. standard deviation) or associated estimates of uncertainty (e.g. confidence intervals)
☐	☒ For null hypothesis testing, the test statistic (e.g. *F*, *t*, *r*) with confidence intervals, effect sizes, degrees of freedom and *P* value noted *Give P values as exact values whenever suitable.*
☒	☐ For Bayesian analysis, information on the choice of priors and Markov chain Monte Carlo settings
☒	☐ For hierarchical and complex designs, identification of the appropriate level for tests and full reporting of outcomes
☒	☐ Estimates of effect sizes (e.g. Cohen's *d*, Pearson's *r*), indicating how they were calculated

Our web collection on statistics for biologists contains articles on many of the points above.

Software and code

Policy information about availability of computer code

Data collection	Viia7 Real-Time PCR System and Perkin Elmer Envision
Data analysis	Excel and Graphpad Prism 7

For manuscripts utilizing custom algorithms or software that are central to the research but not yet described in published literature, software must be made available to editors/reviewers. We strongly encourage code deposition in a community repository (e.g. GitHub). See the Nature Research guidelines for submitting code & software for further information.

Data

Policy information about availability of data

All manuscripts must include a data availability statement. This statement should provide the following information, where applicable:

- Accession codes, unique identifiers, or web links for publicly available datasets
- A list of figures that have associated raw data
- A description of any restrictions on data availability

The datasets generated during and/or analysed during the current study are available from the corresponding author on reasonable request

Field-specific reporting

Please select the one below that is the best fit for your research. If you are not sure, read the appropriate sections before making your selection.

☒ Life sciences ☐ Behavioural & social sciences ☐ Ecological, evolutionary & environmental sciences

For a reference copy of the document with all sections, see nature.com/documents/nr-reporting-summary-flat.pdf

Life sciences study design

All studies must disclose on these points even when the disclosure is negative.

Sample size	We performed preliminary experiments with n=3, n=4, and n=5 to determine the variability between biological replicates in each treatment group. Based on our preliminary optimization, we determined a sample size of 3 replicates was sufficient.
Data exclusions	No data was excluded
Replication	The assays were repeated on three separate occasions to confirm the pattern of regulation and statistical significance presented in the figures
Randomization	We randomized the sample order on the plate in the experiments to minimize the effect of instrument signal drift
Blinding	For performing the cell-based luciferase assay, EC was blinded to the structure of the compounds tested

Reporting for specific materials, systems and methods

We require information from authors about some types of materials, experimental systems and methods used in many studies. Here, indicate whether each material, system or method listed is relevant to your study. If you are not sure if a list item applies to your research, read the appropriate section before selecting a response.

Materials & experimental systems

n/a	Involved in the study
☒	☐ Antibodies
☐	☒ Eukaryotic cell lines
☒	☐ Palaeontology
☒	☐ Animals and other organisms
☒	☐ Human research participants
☒	☐ Clinical data

Methods

n/a	Involved in the study
☒	☐ ChIP-seq
☒	☐ Flow cytometry
☒	☐ MRI-based neuroimaging

Eukaryotic cell lines

Policy information about cell lines

Cell line source(s)	THP-1 cells, human monocytic cell line purchased from Invivogen
Authentication	not authenticated
Mycoplasma contamination	Since cells were purchased from a vendor and used within 20 passages of purchase, we did not test for mycoplasma
Commonly misidentified lines (See ICLAC register)	N/A